Research Square

Preprints are preliminary reports that have not undergone peer review.
They should not be considered conclusive, used to inform clinical practice,
or referenced by the media as validated information.

Rapid Microanalysis-Based Process for Nuclear Material Characterization for Nuclear Forensics

Lori A Metz

lori.metz@pnnl.gov

Pacific Northwest National Laboratory

Brian C Archambault

Pacific Northwest National Laboratory

Matthew Douglas

Pacific Northwest National Laboratory

Samuel B Emmons

Pacific Northwest National Laboratory

Judah I Friese

Pacific Northwest National Laboratory

Benjamin McDonald

Pacific Northwest National Laboratory

Luca Pagani

Pacific Northwest National Laboratory

Matthew A RisenHuber

Pacific Northwest National Laboratory

Sean R Scott

Pacific Northwest National Laboratory

Nicolas Uhnak

Pacific Northwest National Laboratory

Research Article

Keywords:

Posted Date: September 30th, 2026

DOI: https://doi.org/10.21203/rs.3.rs-11054810/v1

License: This work is licensed under a Creative Commons Attribution 4.0 International License.
Read Full License

Additional Declarations: No competing interests reported.

Rapid Microanalysis-Based Process for Nuclear Material Characterization for Nuclear Forensics

L. A. Metz, B. C. Archambault, M. Douglas, S. B. Emmons, J. I. Friese, B. McDonald, L. Pagani, M. A. RisenHuber, S. R. Scott, and N. Uhnak

Abstract

Conventional nuclear forensics workflows rely on complete dissolution and radiochemical separations of bulk samples, providing robust measurements but potentially obscuring microscale heterogeneity and requiring lengthy processing. A complementary microanalysis-based workflow is presented for rapid characterization of nuclear material for nuclear forensics. For post-detonation nuclear forensics samples, the approach integrates radiological particle localization, targeted microsample extraction and gamma spectrometric analysis, automated microdissolution, reduced-volume separations, mass spectrometry, and data-driven process optimization. In two demonstrations, ionizing-radiation quantum imaging detectors identified regions of interest in surrogate post-detonation particulate samples, which were processed by automated microdissolution, custom microcolumns, and multicollector ICP-MS. The experiments demonstrate how uranium, plutonium and neptunium isotopics can be rapidly quantified along with fission products on single particulate samples. The single particulate subsamples showed distinct isotopic compositions, demonstrating heterogeneity that bulk analysis would obscure. These results establish a targeted microanalysis pathway that complements established bulk methods and supports adaptive processing and streamlined reporting.

Introduction

Nuclear forensics is the characterization of interdicted nuclear materials or devices found outside of regulatory control and post-detonation nuclear events (Figure 1). It assists law enforcement and intelligence agencies in preventing, mitigating, and attributing a nuclear or radiological event (NAS 2010). In the U.S., the nuclear forensics process is accomplished by using multi-disciplinary technical teams across U.S. government agencies and national laboratories (Metz 2025).

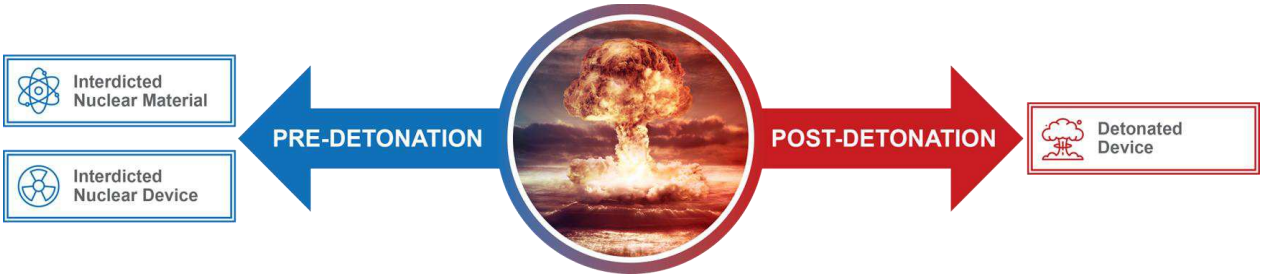

Figure 1. Nuclear forensics involves the characterization of pre-detonation interdicted nuclear material and devices as well as post-detonation nuclear events.

Sample processing and analysis is extremely challenging as samples are valuable and can be difficult to collect. The chemical and radiological nature of the samples are complex, especially for post-detonation samples that consist of a mix of fission products, activations products, actinides, and environmental constituents. Laboratory analysis of post-detonation nuclear forensics samples consists of quantitative analysis for isotopes of many elements. The quantitative analytical measurements require methods capable of a large dynamic range of analyte levels and half-lives. Technical integrity must be robust as results from analytical methods are used in high-consequence decision making. Due to these challenges, the overall analysis process relies on a very robust bulk analytical process. In most cases, the entire bulk samples are completely dissolved as received. The dissolved sample is then taken through a series of steps, including chemical separations and purifications, to ensure all analytes are quantitively and accurately measured. Figure 2 outlines the steps that are involved in the laboratory radiochemical analysis of both pre-detonation and post-detonation samples.

The nuclear forensics nuclear material analysis process is set up for receiving samples from material and device interdictions and collected ground and air debris from a detonated nuclear device. The samples are non-destructively screened when they first arrive at the laboratory to obtain some rapid, early forensics information and to triage and prioritize them to determine if they will proceed to destructive analysis. If the sample is selected for destructive analysis, then the whole sample or a portion of the sample undergoes complete dissolution/decomposition for quantitative analysis of a suite of analytes. Additional measurements are made immediately following dissolution to provide some more forensics information and to help plan the aliquot sizes and sequence of chemistry steps for each sample to optimize for time and to meet data quality objectives. Elemental separations are performed to separate out interferences before being analyzed by mass spectrometry and radiation detection methods to obtain final reported results. The simplified circle figure (Figure 2) suggests reporting only takes place at the end of measurement of separated fractions, but in fact data is analyzed and reported throughout the process with appropriate measurement uncertainties. For more information about this process please see Metz et al. 2025.

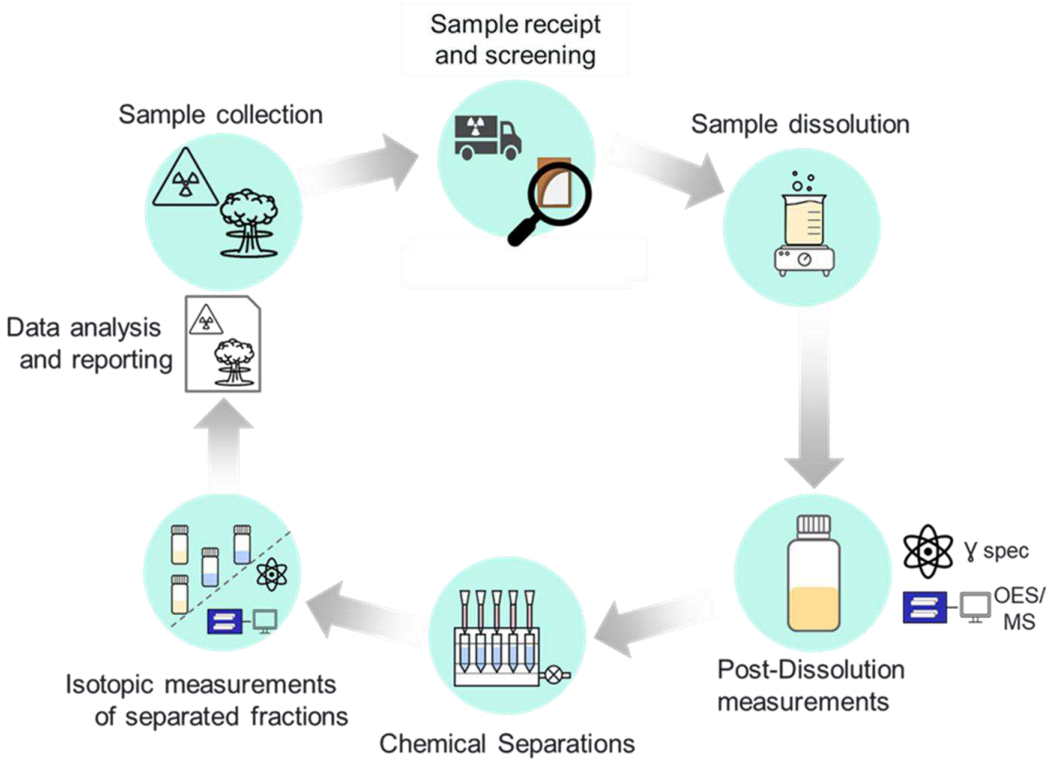

Figure 2. Current nuclear forensics laboratory analysis process (Metz 2025).

The current work discusses a new process that could quickly identify microregions (or smaller) within a sample that could be extracted and analyzed as new microsamples, potentially greatly speeding up the process for some of the analytes of interest. The new process described here is not meant to replace the current robust bulk nuclear forensics process but rather create an optional rapid parallel analysis pathway for some analytes of interest that may vary for the given nuclear event. It is envisioned that a parallel microanalysis approach could help both pre-detonation and post-detonation nuclear material analysis, but this initial paper focuses on research for analysis of post-detonation samples. Developments from this work can also help optimize microanalysis processing for many other analytical applications.

New Process Concept

The primary goal of the current work is to develop a new analytical processing flow specifically designed for nuclear forensics samples. The new workflow rapidly selects microsamples within a bulk sample to reduce sample mass and reagent volumes processed through chemistry, streamlining the analysis of some analytes (Figure 3). For post-detonation samples, the goal is to select a suite of microsamples within the bulk that are concentrated in nuclear debris. Post-detonation samples as collected consist mostly of environmental material with trace amounts of nuclear debris. Extracting concentrated subsamples can reduce the unwanted background material and potentially speed up the

overall nuclear material analysis process as a result of minimizing the sample mass. To further optimize this microanalysis processing flow, we are developing chemistry models that can learn from early time data to autonomously optimize processing steps. Also, research involves AI/ML assisted data analysis to reduce the need for expert involvement and signal when data are ready to be reviewed and reported.

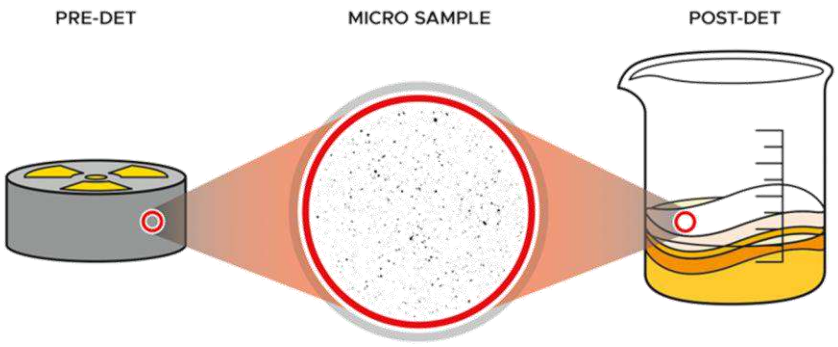

Figure 3. Smaller, targeted sample sizes and real-time process optimization can reduce laboratory analysis timelines by measuring a prioritized set of samples.

The envisioned new analytical process very quickly locates particulate from the event in the air filter or ground sample, extracts and potentially combines the particulate to form new microsamples, gamma counts the new samples so all measurements can be ratioed to the number of fissions represented in the samples, and then sends the new samples through a series of microchemistry columns prior to isotopic measurements by mass spectrometry and radiation detection. Measurements that are made at each step of the process will be fed into chemistry- and physics-based models that will determine which additional steps are needed to remove the measurement interferences for the priority isotopes for the specific event scenario. Models will also be used to assist in data analysis and determine when measurement requirements for a given priority analyte are met, and the data can be reported. This feedback loop with measurements being taken after each processing step and incorporated into optimization models has the potential to greatly reduce processing time by only selecting steps that are needed for the given analysis scenario. Figure 4 depicts this new integrated analytical process. To develop this new process research is being conducted in 4 main areas as depicted in Figure 4: locating/in situ analysis of event particles, rapid particle extraction/microchemistry, real-time process optimization, and AI/ML assisted measurement/reporting.

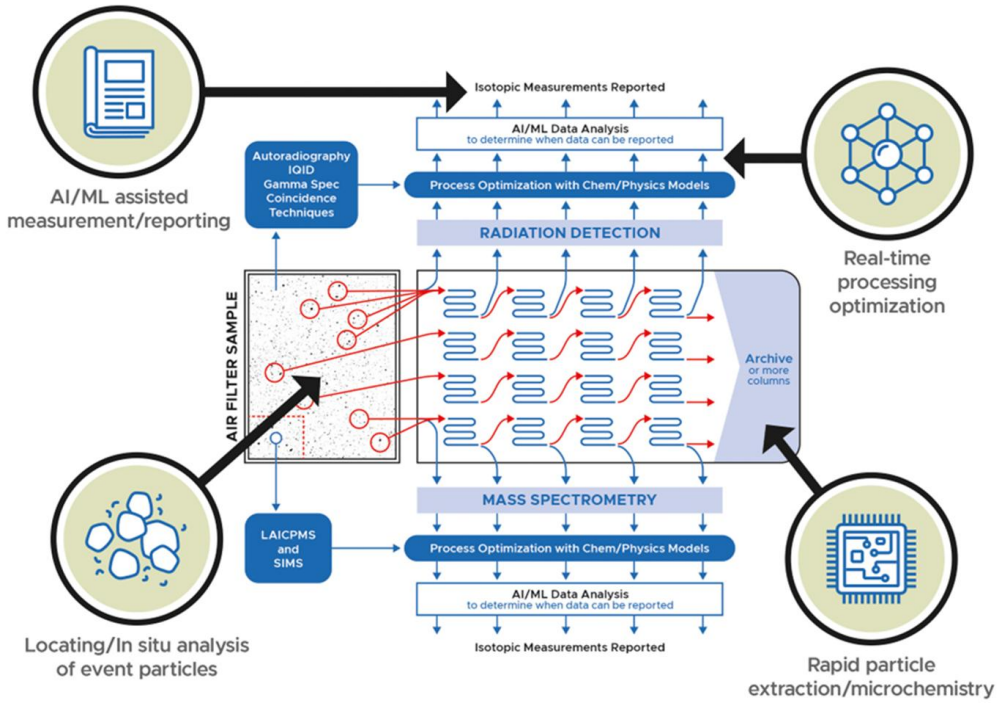

Figure 4. The envisioned new microanalysis process for nuclear event characterization.

Locating/In situ analysis of event particles

Experiments are being conducted to evaluate different radiological and physical properties of nuclear debris that can be used to rapidly locate debris particulate of interest. For radiological properties, the work focuses on developing methods that use advanced digital autoradiography systems to identify particles of interest in samples with large fission product emissions throughout the sample. In particular, experiments are assessing the performance and applicability of ionizing-radiation Quantum Imaging Detectors (iQIDs, Miller 2014) and large-area CCDs. Investigations also involve using collaborative robots for scanning large samples with the iQID and then marking regions of interest. To characterize physical properties, optical microscopy is used to catalog samples by color, shape, and size, and by electron microscopy for morphological and elemental analysis. Gathering information on a number of samples will help show whether there are unique properties that can improve the probability of rapidly selecting samples with higher concentration of analytes. The biggest research challenge within this area is ensuring that the methods can work well under a range of potential radiation levels and sample types. For example, if the sample is received within days of the event, it will have a much higher total radiation level than if it is received weeks or months later. It is also important to make sure these methods (and subsequent methods) can in fact be performed rapidly because that is one of the primary purposes of the parallel process – rapid meaning faster than the current bulk analysis process. Emphasis is therefore placed on methods compatible with automation.

Because the concept demonstration illustrated later in this manuscript involves the use of the iQID, more information on the system is provided here. The ionizing-radiation quantum imaging detector

(iQID) describes a range of custom prototype and commercially available intensified camera systems for real-time digital autoradiography. An iQID couples a plastic scintillator screen to an image intensifier. The scintillation light clusters produced by ionizing radiation interactions are recorded by a camera as processed list-mode event data. Key characteristics include high spatial resolution, coarse energy resolution, particle discrimination, high count-rate capability, and minimal sample preparation requirements. These systems have found wide use in medical research (e.g., targeted alpha therapy), microdosimetry studies, and security related research. A wide range of suitable scintillators materials and adjustable parameters make iQID a flexible system for nuclear forensics as well.

Some initial results from this research are provided in the Concept Demonstration section later in this paper. Additional results are found in citations listed below (McDonald 2026 and Patz 2026) and future publications in process.

Rapid particle extraction/microchemistry

Once the particles of interest are found, methods are being developed to extract the particulate or groups of particulate, transition to a microchemistry platform for dissolution and separations, and followed by analysis using radiation detection or mass spectrometry. Experiments are being conducted to evaluate automation-capable platforms and methods for rapid dissolution of large numbers of particles, prepare samples for liquid chemical separation, and then perform fast small-scale group separations. Investigations utilize a commercial off-the-shelf device to dispense acids via a GUI system and heating/shaking capability to help facilitate 'hands off' particle dissolution. Disposable parts such as sample holders and microchemistry columns are custom designed and 3D printed to optimize micro separations and movement between steps. Method development initially focuses on actinide micro separations and analysis by ICP-MS using extraction resins (e.g., Eichrom) to facilitate rapid separations. Experiments are also being conducted that could potentially remove particulate directly off a substrate with a solvent stream like what is used in nanospray desorption electrospray ionization (nano-DESI) technology (Roach 2010). One of the biggest challenges involved in this research area is to demonstrate that the rapid microchemistry methods are capable of adequately quantifying the target analytes at the lower levels found in the microsamples. Some initial results from this research are provided in the Concept Demonstration section of this publication. Additional results are being prepared for future publications.

Real-time process optimization

A predictive chemical model (RALF: Rapid Analytical Laboratory Flowsheet) is being developed based on historical separations data that will provide targeted chemical separations methods. The historical separations data results from more than 50 campaigns of processing and analyzing irradiated materials for both operational readiness exercises, as well as R&D aimed at improved separations and updates to nuclear data, that have been accumulated into a database. These separations have either been robustness-tested through significant validation and verification efforts or are planned to be. The database contains all pertinent information required to accomplish the

separation, including acid concentration and matrix (e.g. HCl or HNO_3), loading and elution volumes, resin material, results including chemical yields, and contaminants.

PNNL separations schemes are based on a sequential separation that maximizes the number of analytes that can be quantified from a single aliquot of sample and are based on extraction chromatographic resins. Examples of these separations can be found elsewhere (Morley 2015, Herman 2024). Results in the database are accumulated from the irradiation of an actinide target with various neutron energies including thermal, fission, and 14 MeV; targets include highly enriched uranium, depleted uranium, as well as transuranic actinides. Each of these campaigns are the results of dozens of chemists, radiation spectroscopists, and physicists, separating and analyzing actinides, fission products and activation products using numerous analytical methods.

There are several conditions required for the working model for the purpose of operational post-detonation nuclear forensics. First, it must be robust and simple, must not have a software license mortgage, and must operate without the need to connect to the internet. These caveats directed the work towards a python-based program that operates outside of the internet, on an internal server, while also not requiring a significant compute cost. At a high level, the RALF: 1) processes early time data inputs including gamma and elemental data, 2) converts that machine readable information into a user interface that allows the user to select elements through a custom GUI, 3) parses the database converted to a machine-readable format and provides a suggested separations scheme that minimizes time to isolate those individual elements. A diagram of this process is shown below in Figure 5, where a generic separation flowsheet is shown with RALF optimized streamlining applied. Time is calculated based on an estimate of the time required for a given step, e.g. a vacuum aided chromatographic cartridge separates at 1 mL/min, therefore loading 20 mL on the cartridge would take 20 minutes to progress. The time cost-comparison means that separation schemes that require a significant number of matrix transpositions, that require large volumes, or digestions, are eliminated.

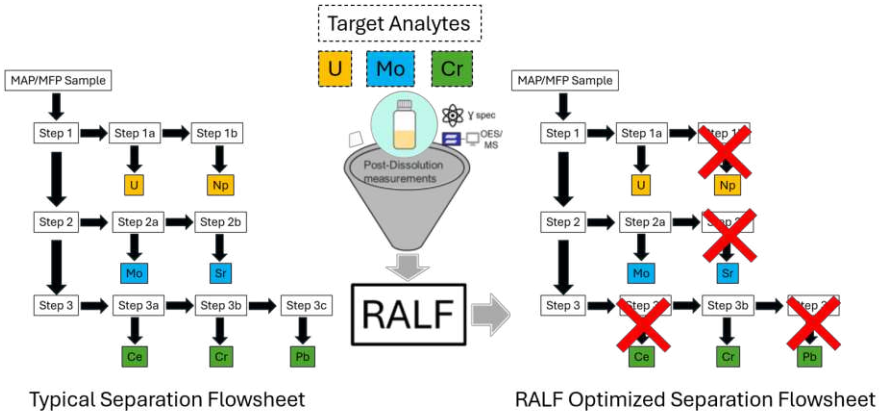

Figure 5. Diagram of the workflow for RALF, generic flowsheet is shown. MAP/MFP: Mixed Activation Product/Mixed Fission Product, a generic term for a forensics relevant sample matrix.

As a consequence of separations data originating from a sequential process, eliminating a given step upstream may create unintended interferences in the final fractions. To address this issue a custom gamma interference cross-check script has been developed that takes the potential separation final fractions and compares the gamma emissions from the radionuclides within that fraction to determine if there are interferences. If an interference is found RALF conducts a purity evaluation to determine how much of the interference can be present to quantify the analyte of interest in the presence of the interference. RALF then prompts the user to make a choice on whether the suggested scheme is acceptable. If deemed unacceptable then a secondary separation scheme is suggested that eliminates that issue. To address potential unknown separation behavior for elements that have little to no data, a thermodynamic based chromatographic predictor using the MOOSE program is incorporated. This will provide separation prediction, particularly important for other concerns such as weak radiation emitters, or high quantities of stable materials. A validation effort is planned, using a select number of analytes that have high impact to a nuclear forensic evaluation.

Multi-physics computational chemistry modeling is being conducted to understand the fundamental mechanisms where thermodynamic data is not available for certain separation conditions. Building up from quantum calculations, molecular dynamics simulations, up to thermodynamics such as aqueous stability constants allows prediction of chemical behavior starting from first principles. The lack of data on thermodynamics is a big major research challenge in this area, bridging this gap has been a concerted effort. Results from this work can be found in the citations below (Hadi 2025, 2026), comprising many forensics elements as well as the entire lanthanide series. These efforts highlight a need in applied science that can be addressed using computational science where the basic science would be onerous and expensive to complete.

The microanalysis concept demonstrations discussed below do not yet include aspects of this research, but they will be incorporated in future demonstrations to enable real time process optimization.

AI/ML assisted measurement/reporting

Classifying high-resolution gamma spectra by their isotopic content is essential to nuclear forensics, yet traditional analysis methods are time-intensive and require extensive expert review. To address this challenge, we developed machine learning (ML) approaches that leverage analyst-reviewed, historic data from high-purity germanium (HPGe) detectors to automate nuclide identification (NID).

Using approximately 1,600 well-labeled experimental gamma spectra covering 65 unique isotopes, we used supervised ML to train gradient boosted decision trees (XGBoost) and deep neural network (DNN) classifiers that significantly outperform traditional commercial software. For example, in the case of Cd-109 (a challenging isotope due to multiple possible interferences), ML models dramatically reduced false positives while producing minimal false negatives in comparison with Miron's Genie 2000 gamma spectroscopy software (G2k). ML model precision in that case was 100%, whereas G2k only achieved 45%.

Overall, these models outperformed the NID methods of G2k primarily by producing far fewer false positives while maintaining comparable false negative rates. During model development, the best model achieved an F1 score (metric balancing false positives and false negatives) of $F1 = 0.97$, while G2k achieved $F1 = 0.84$ on the same development dataset. Further, when making predictions for an independent test dataset of 123 gamma spectra produced in recent R&D, the best model achieved an overall $F1 = 0.92$, while G2k achieved an $F1 = 0.80$. To build trust in these automated predictions, we applied Shapley Additive Explanations (SHAP) to demonstrate that model decisions are grounded in physically relevant photopeaks and spectral context, such as parent-daughter isotope relationships or isotopes that behave analogously during radiochemical separations. Details of the development of the dataset, chosen architecture, and a discussion on the implementation and effectiveness of these techniques are presented elsewhere (Emmons 2026).

Examples of the application of these models in the context of the micro-analysis demonstration are shown in Figure 6. The SHAP explanations for the positive identification of Rh-106 from the gamma spectra of the whole filter sample during screening are shown on the left, illustrating that the ML model leveraged presence of both the 621.9 keV and 512 keV peaks to identify the presence of Rh-106. The SHAP explanations for the positive identification of Nb-95 from the gamma spectra from one of the particles (pre-dissolution) are shown on the right, illustrating that the ML model leveraged the presence of both Nb-95's 765.8 keV photon and the presence of its parent nuclide Zr-95 by its 756.7 keV photon.

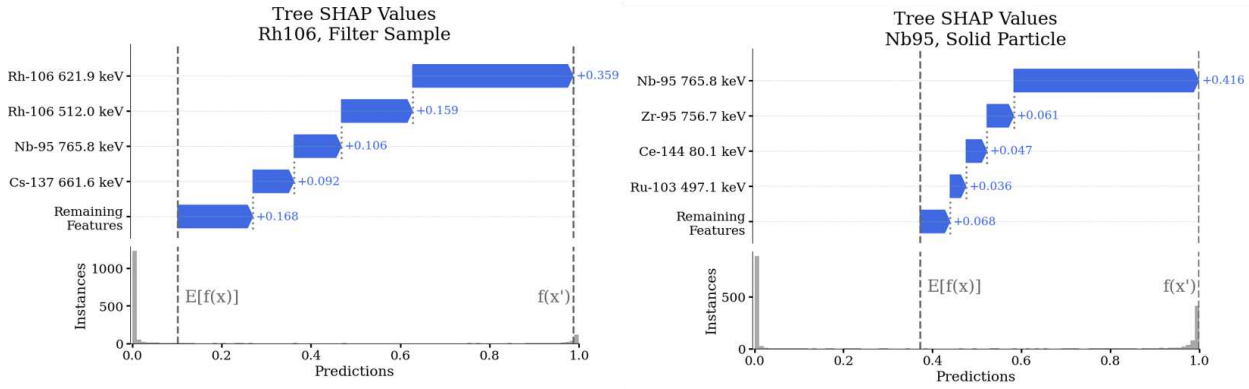

Figure 6. Select nuclide identification results from the XGBoost model and their respective SHAP interpretations.

Complementing this supervised approach, the team also developed dense autoencoders to compress and organize unlabeled gamma data into latent representations, enabling efficient characterization. By clustering encoded spectra and removing over-abundant data categories, they achieved more balanced datasets and improved model performance. Results from this effort can be found in the citation below (Lonsway 2026). Together, these advances establish a practical automated "spectroscopist-in-the-loop" analysis process that scales easily to enable near real-time analysis of the

hundreds of gamma spectra required for this rapid micro-analysis approach to be successful. The microanalysis concept demonstrations discussed below do not yet include aspects of this research, but they will also be incorporated along with predictive chemical model (RALF) in future demonstrations to further streamline the analysis process.

Concept Demonstration

Sample description and processing flow

Two demonstration experiments were conducted to facilitate the development of this new microanalysis process. Sol-gel samples that were previously prepared as part of the development of post-detonation nuclear debris surrogates (Lusk 2023, Diehl 2024, Snow 2025, Cooper 2025) were used to connect the following individual methods developed as part of this research: locating event particulate, particle extraction, and microchemistry. The first experiment utilized sol-gel particles ~ 1 mm in diameter containing weapons grade Pu and fission products. The fission products were produced from the irradiation of a depleted uranium target as previously described (Lusk 2023). The uranium target material was separated from the fission products before loading the fission products onto the sol-gel particulate as previously described (Lusk 2023). The batch of particulate was loaded with a solution containing 1E+13 fissions total. With 10 ppb Pu-239, each particle contained ~8 mBq of Pu-239. When the samples were measured by the microanalysis process it had been ~7 months after the photofission irradiation (April 24, 2025), so many fission products had fully decayed. As a point of reference, the measured contact dose rate for the particles was 9.2 mR/hr (open window) on September 4, 2025. Figure 5 provides a flow diagram of the steps that were followed in the first experiment.

The second experiment analyzed sol-gel particles that were ~50 um in diameter and contained fission products. As with the sol gel material described above, the fission products were produced from the irradiation of a depleted uranium target, and the target material was separated from the fission products prior to loading on the particulate. The batch of particulate contained 2E+12 total fissions. When the samples were analyzed by the microanalysis process it had been ~17 months after the production of the fission products (July 17, 2024). The particulate was on a Whatman filter that was used to swipe an area in the sample preparation location known to have sol-gel particles. Figure 7 provides a flow diagram of the steps that were followed in the second experiment.

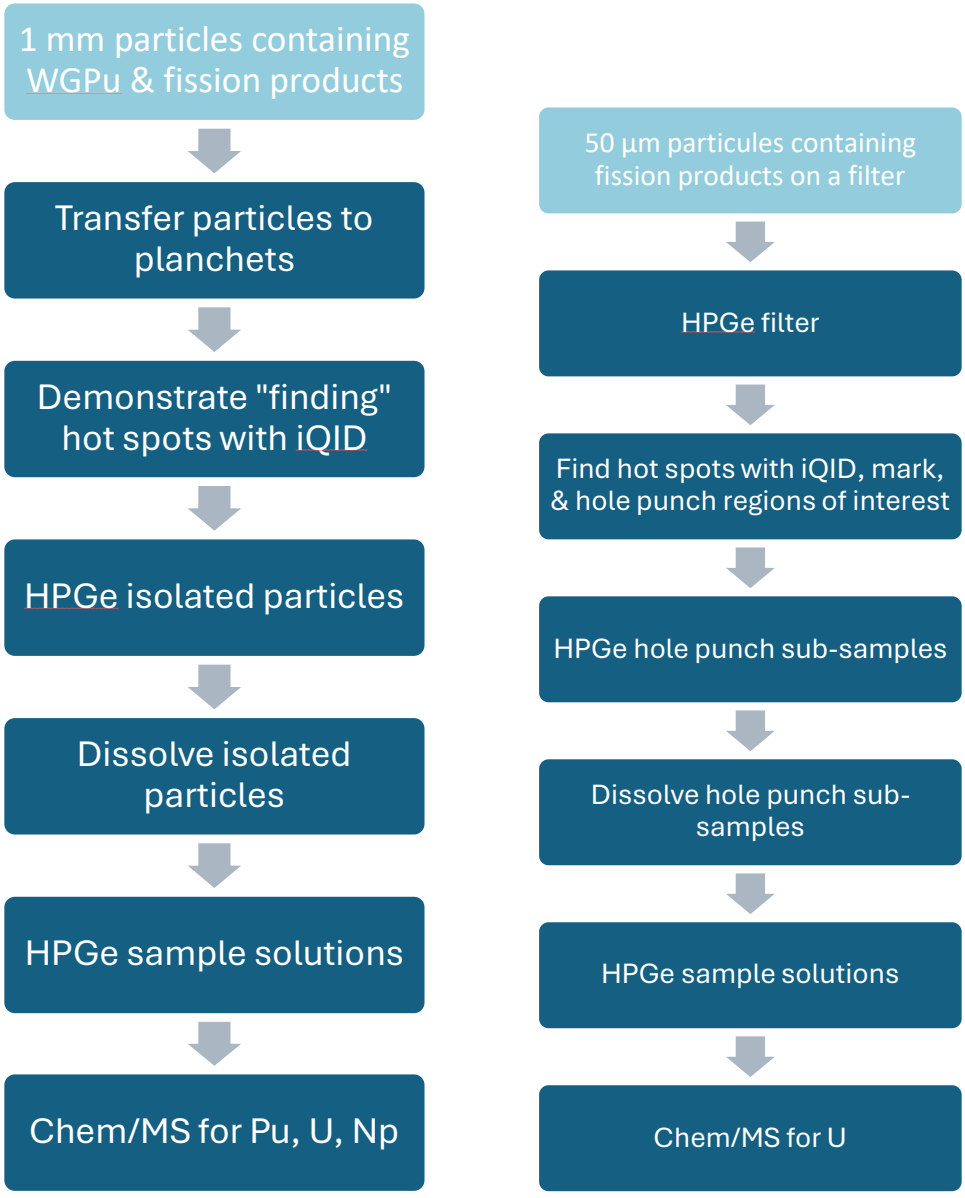

Figure 7. The flow charts on the left and right show the steps followed in the first and second demonstration experiments, respectively.

Locating particles or regions of interest

For the first experiment, a set of ~ø1 mm particles were picked and placed onto stainless steel planchets coated with double sided tape with either one, two, or three particles placed per disk. As an initial experiment, we chose not to add other matrix constituents to the planchet to challenge finding these particles of interest within background particulate (since these particles were visible with the naked eye). Nonetheless, the experiment served as an initial evaluation of the steps involved in the microanalysis process before moving to more complex sample types. These were then

covered with 3.6 μm-thick mylar (Chemplex) to encapsulate the particles while minimizing alpha attenuation. The discs were counted via HPGe, enabling quantification of several long-lived fission products, and then were measured via iQID (Figure 8).

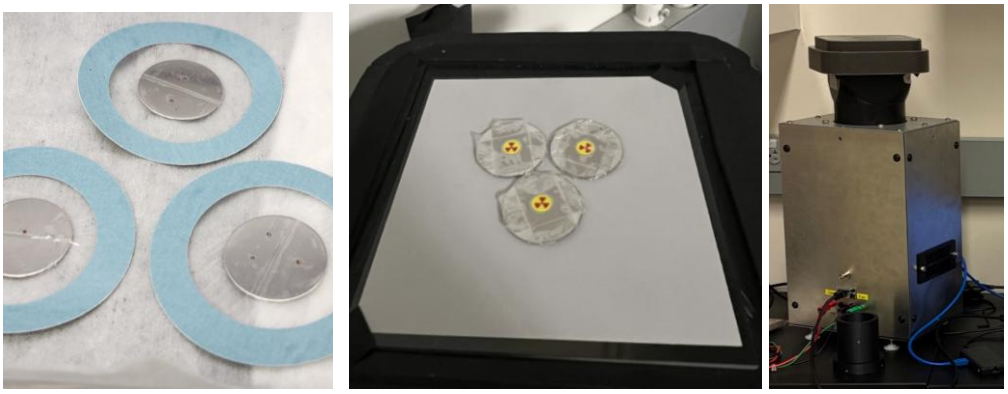

Figure 8: (Left) Photo of particle samples on steel planchets used for the first experiment. (Middle) Samples facing EJ-444 scintillator on iQID imaging surface. (Right) Photo of 10 cm x 10 cm iQID system.

Measurements were conducted with an EJ-444 0.15mm-thick scintillator, the image intensifier at 0.7 V, and considering a maximum cluster size of 11x11 pixels with an intensity threshold of 30. The three planchets were measured simultaneously for 60 hr. The autoradiograph (both centroid and cluster images) shows respectively one, two, and three hot spots corresponding to particles 1 on top, 2 and 3 on the right, and 5, 6, and 7 on the left (Figure 9).

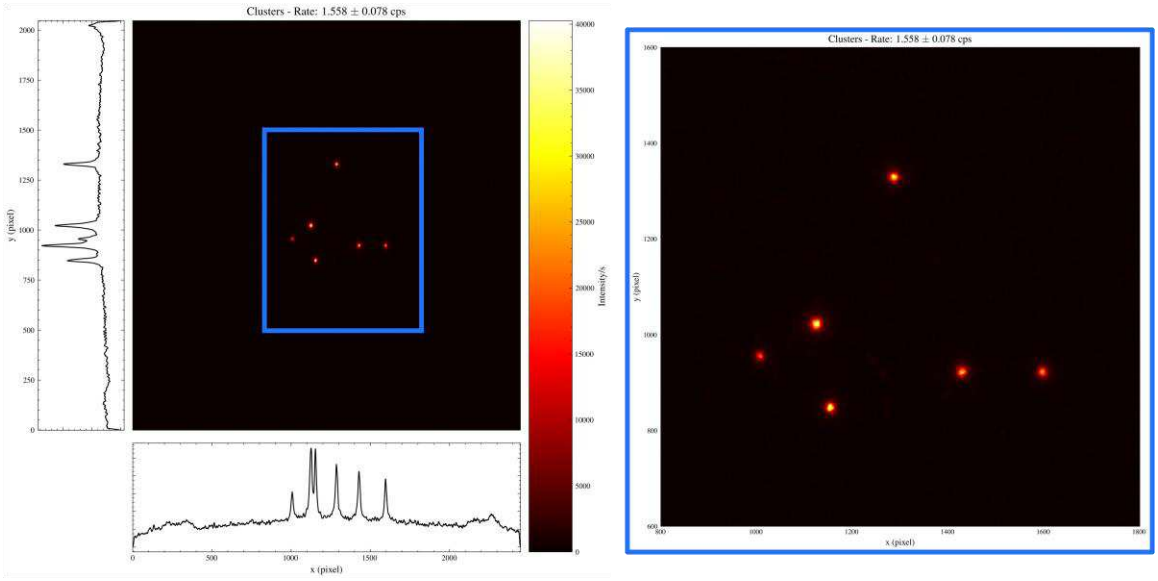

Figure 9: (left) iQID cluster image showing the radiograph of the 6 particles. (right) Zoom in showing 1 particle on top, 3 on the left, and 2 on the right.

For the second experiment, the smaller ~50 μm particles collected on the filter paper were first analyzed via HPGe. The filter paper was then placed into a plastic weigh boat that had been trimmed to form a plastic circle for structural support. The back of the plastic support was coated with single-sided adhesive Kapton tape that protruded outside the area of the support. On top of the assembly, a single layer of mylar was placed so that it both held the sample down and contacted the sticky side of the Kapton to encapsulate the sample. The encapsulated filter with particulate was then measured on the iQID by placing the mylar-covered side of the filter in contact with the plastic scintillator.

Measurements were conducted with an EJ-444 0.15mm-thick scintillator and with the same hardware settings used to measure the larger particles. The sample was counted for 60 hr. The autoradiograph (Figure 10, both centroid and cluster images) was used to determine regions of interest (ROIs). With reference to Figure 10, six ROIs were considered: three with elevated activity or signal (labeled 1, 2, and 4), and three with background activity levels (labeled 3, 5, and 6).

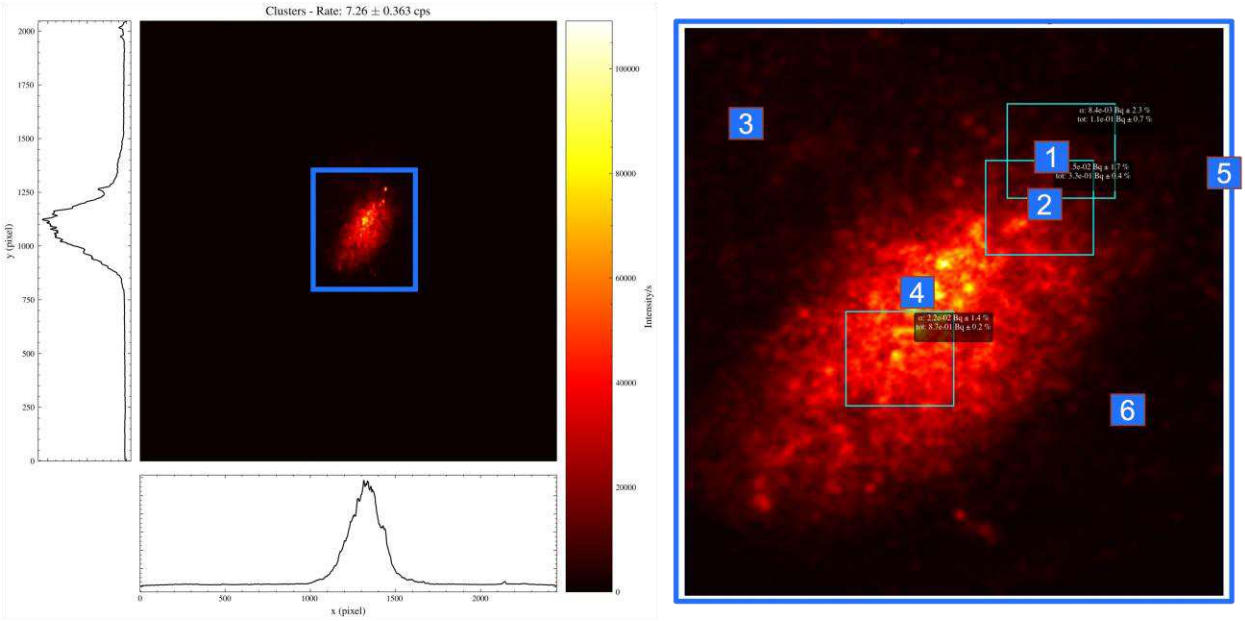

Figure 10: (left) iQID cluster image showing the radiograph of the small particles sample. (right) Zoom in showing the 6 identified ROIs.

Gamma counting and dissolution

Prior to conducting the first experiment, dissolution, chemistry, and mass spectrometry evaluations were conducted on the larger, 1 mm, particles as received. A total of eight single particles were picked and placed into 6 wells of a 96 – place well plate. Five of the eight particles were dissolved as single samples and the last three particles were combined as a larger sample. These were then placed into a Hamilton Micro-Lab Prep and had 15 μL of concentrated nitric acid (HNO_3), 10 μL of concentrated hydrochloric acid (HCl), and 10 μL of concentrated hydrofluoric acid (HF) pipetted

onto them. All acids were of OPTIMA grade from Fisher Scientific and were pipetted using Hamilton's CO-RE®-II conductive filtered tips. The particle samples were heated at 100°C and shaken at 1000 rpm on the Hamilton Micro Lab Prep's Heater Shaker until dry, ~2.5 hours. Residues from the dissolved particles were then brought up in 3 M HNO_3 before proceeding to chemistry.

For the first experiment, the picking, placing, and initial counting of the particles used are described in the previous section. After being analyzed via iQID, the planchets were cut using tin snips so that each particle was isolated and they were each counted individually via HPGe. After the HPGe count, they were each placed into wells of a 96-place well plate and dissolved in the same manner as described in the preceding paragraph. Once dissolved, each sample was transferred into a secondary vessel with 3 M HNO_3 to be recounted via HPGe to determine any sample loss. They were then once again transferred with 3 M HNO_3 back to the well plate and dried down before proceeding to chemistry. During this experiment, it was determined that actinide tracers (e.g., 233U, 244Pu) need to be added prior to dissolution to ensure equilibration and accurate quantification of actinides.

The activity of peak yield fission products was monitored within the particles in order to assess their recovery following dissolution. Mean recoveries ranged from 70-80%, however due to the age of the particles at the time they were processed and analyzed, activities were low and uncertainties may not have adequately captured the true range of activity. While no undissolved material was visible, we will continue to monitor recoveries in future work.

In the second experiment involving the smaller sol-gel particles on filter paper, the analysis from iQID was utilized to determine ROIs from which to obtain subsamples. Six different regions were sampled from the filter paper using a 3 mm hole punch as seen in Figure 11. These cuts were placed into ½ dram vials, Figure 11, and reanalyzed via HPGe. The hole punches were placed into custom designed 3D printed vials that fit within a 96-plate well plate, also custom designed. These vials are printed from Formlabs High Temperature resin to allow for heating without any structural damage. In addition, an added benefit of these vials is that the samples can be counted, dissolved, and recounted without any transferring of samples between different types of containers. Reduction of analytical timelines and sample loss is achieved using these vessels.

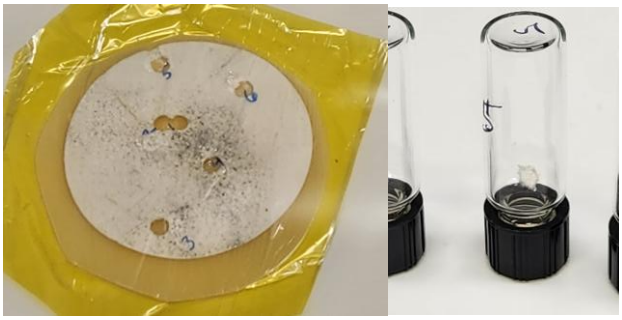

Figure 11. (Left) small particle sample with hole punched areas of interest. (Right) hole punched sample in vial.

Microchemistry and mass spectrometry

A microchemistry separations sequence has been developed based on a larger format chemical separation performed for the bulk nuclear forensics analytical process (Richard 2026). Rather than using Eichrom resin cartridges containing 1 or 2 mL of resin, 3D printed columns that are compatible with the 96-place well plate design used by the liquid handler are used. Each column assembly contains 8 individual columns with a resin bed volume of 0.1 mL. Once samples are ready for chemical separations, individual sample vials are placed within the liquid handler in the 3D printed 96-place well plate. Samples are redissolved in 0.1 mL of 3M HNO3 + 10 % H2O2, and allowed to equilibrate for ~ 5 minutes. Columns are conditioned with 3M HNO3 + 10 % H2O2, then samples are loaded by the liquid handler. The 8-position column assembly is moved across a 3D printed bracket that holds the columns above a 96-place well plate with 2 mL reservoirs. After the automated loading and washing the columns with 3M HNO3 + 10 % H2O2 are completed, individual fractions of Pu, Np, Th, and U are collected in the well plate. After chemistry, the well plate is directly transferred to the autosampler of the mass spectrometer for analysis.

All actinide measurements were completed on a Neoma MS/MS MC-ICP-MS attached to an ESI SC-uDX autosampler. An ApexOmega desolvating nebulizer and Jet/X cones are used to improve sensitivity and provide ion yields on the order of 2 %. The well plate containing the actinide fractions is placed directly in the autosampler, and the respective fractions are analyzed directly without any dry downs or transpositions, which is necessary to achieve rapid timeline targets. Analytical methods vary depending on the analyte and the final concentration in the separated solution, and generally involve the use of the "nuclear package" ion counting system that includes a series of secondary electron multipliers, compact discrete dynodes (CDDs), and Faraday cups. Detector yields are determined at the beginning of an analytical session, which can be accomplished prior to and/or during the microdissolution and microchemistry procedures. When U contents are relatively low, the same cup configuration can be used across all analytes such that Pu, Np, and U can all be analyzed in sequence without human interference of the mass spectrometer after initial setup. However, when U contents are relatively high (requiring, for example, that ^{238}U be measured on a Faraday cup), the sequence must be interrupted to move a Faraday cup or CDD into the correct position. The total process, from chemistry to mass spectrometry analysis, can be achieved in a matter of hours per 8 samples (see Richard et al. 2026 for details on timelines).

Methodologies described above underwent significant iterations during their development, which culminated during the two demonstration experiments described in this paper. Table 1 provides Pu and Np isotopic composition data for a set of the larger sol-gel particles containing fission products and weapons grade Pu from the first experiment. Total atoms of ^{237}Np and ^{239}Pu were quantified, as well as the ^{240}Pu/^{239}Pu and ^{237}Np/^{239}Pu. This set of samples were used to test the Pu tracing methods using a ^{244}Pu tracer; half of the samples were spiked pre-dissolution, and the other half post-dissolution. Total atom amounts for ^{239}Pu were determined by both isotope dilution and external calibration assuming the average chemical yield determined in previous experiments for Pu (55.9 ± 7.1 %). This allowed for comparison between the two quantification methods, and demonstrated the

need to add tracers prior to dissolution to ensure equilibration between tracer and sample. ^{237}Np total atom amounts were determined by external calibration assuming the average chemical yield determined in previous experiments (32.4 ± 2.9 %). Atom amounts were corrected for total processing blanks that accompanied the samples.

Pu fractions from the microchemistry are collected in 0.55 ml of 3M HNO_3 + 0.01M ascorbic acid. Direct analysis of these fractions is the goal and is the defining volume for determining the amount of ^{244}Pu tracer to add to each sample to provide an adequate beam intensity on the mass spectrometer. In the case of the large Pu sol-gel particles, the Pu contents were significantly higher than expected, which required samples to be diluted prior to analysis. This resulted in a lower than ideal count rate on ^{244}Pu and high uncertainties on the resulting ^{239}Pu quantification by isotope dilution. Overall uncertainties for atom quantification by external calibration were better, on the order of 7 % for ^{239}Pu. Good agreement was obtained between the yield corrected external calibration atom quantification and isotope dilution values (within 5 %) for particles in which tracer was added before dissolution. Given this good agreement between the two quantification methods, the goal of obtaining reasonable uncertainties (5 % or less) on a rapid timeline is possible.

Np fractions were collected in 0.55 ml of 2M HNO_3 + 0.01M oxalic acid, which would again provide a determining volume for tracer additions. For these experiments, an adequate ^{236}Np tracer was not available, leaving only an external calibration measurement. Previous experiments gave more consistent, albeit rather low, yields for ^{237}Np. Like Pu, a high amount of ^{237}Np was present in the samples and required dilution for analysis. Even with all known sources of uncertainty, the ^{237}Np uncertainties were slightly lower than that of ^{239}Pu, on the order of 4 – 5 %.

Isotopic ratios were clustered around values of ~0.022 and ~0.1 for the ^{240}Pu/^{239}Pu and ^{237}Np/^{239}Pu, respectively. One particle deviated from this main cluster, with a ^{240}Pu/^{239}Pu of ~0.035 and ^{237}Np/^{239}Pu of ~0.068. This particle also had higher ^{239}Pu atoms than the other particles, showing a clear additional source of Pu contributing to its isotopic composition. These data show that analysis at the scale of investigation can provide information on the heterogeneity present within a series of samples that are otherwise assumed to be homogeneous. For example, if these particles were mixed with a soil and processed as a bulk sample, any information about inter-particle heterogeneity would be lost.

For the second demonstration experiment, punch outs from the filter paper (Figure 12) were dissolved and measured for uranium isotopic composition. As described in previous sections, punch out locations were chosen based on the iQID imaging, and included three "hot" spots, and three additional spots that did not show activity on the iQID but were variously "dirty" based on visual inspection. These samples were not traced with a ^{233}U tracer and were used to test the microdissolution and chemistry methods on a "filter" type of sample without any physical separation of the particulate from the filter itself. The particles that were assumed to be captured on this filter paper were not known to contain any uranium (the uranium target material had been removed from the mixture of fission products during preparation of the sol-gel materials). Although a tracer was

not used to quantify the uranium present in each sample, the total amount of uranium recovered from the microchemistry was determined by external calibration.

Uranium isotopic compositions, including $^{234}U/^{238}U$, $^{235}U/^{238}U$, and $^{236}U/^{238}U$ were unique for each individual punch, with total U recovered ranging from ~1.3 (same level as the total process blank) to ~7700 pg per punch (Table 2). Five of the six punches contained enough U for isotopic analysis, and each punch contained an isotopically unique composition that reflected a mixing trend between two distinct uranium reservoirs (Figure 5), with $^{235}U/^{238}U$ ranging from ~0.021 to 0.097. This mixing trend was not consistent with a natural uranium endmember. There was no relationship between the amount of uranium and the isotopic composition. The key finding of this analysis is that if this sample were to have been processed as a bulk sample (i.e., the entire filter dissolved and analyzed), a single isotopic composition would be measured. Subsampling the filter provided unique insight into the heterogeneities present within the sample, which possibly varied due to past processing activities within the fume hood where the swipe was collected.

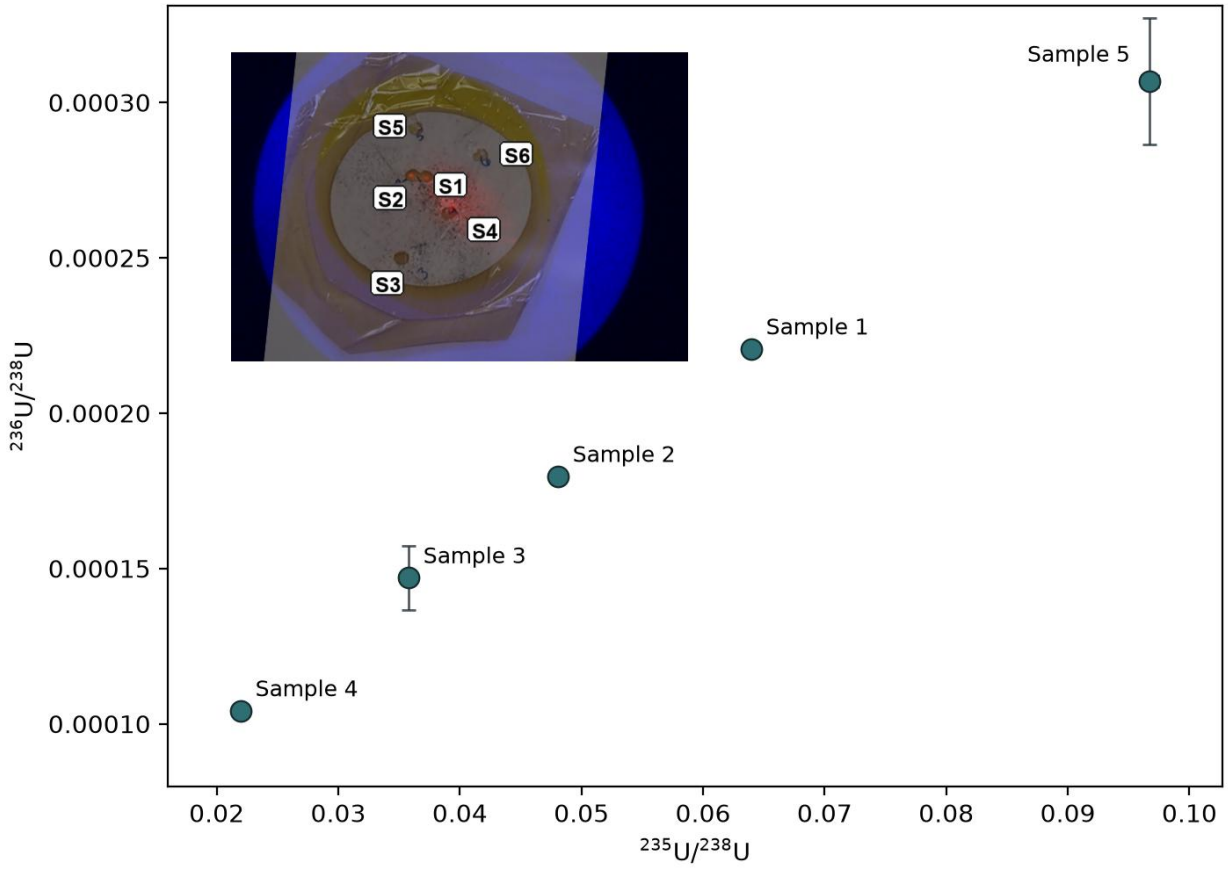

Figure 12: Uranium isotopic compositions of ø3 mm punch samples from small particle filter. Sample numbers also correspond with the labels on the autoradiograph image in Figure 10. Sample 6 did not contain U above process blank levels (~1.5 pg).

Conclusions and Next Steps

A new microanalysis-based process has been demonstrated to streamline some of the key measurements needed for nuclear forensic materials analysis. Rapid quantification of fission products and actinides is possible using the described microchemistry process. To quantify actinides on a fission basis for nuclear forensics, use of 3D printed vessels allows for easy transfer of samples between gamma spectrometry and liquid handling platforms. Quantification by isotope dilution, generally accepted as the most precise method, requires careful consideration of elution volumes and tracer quantities needed to obtain adequate uncertainties, as well as isotopic mixtures that will allow for quantification of multiple actinides simultaneously. The key result of experimental work presented here is the observation of heterogeneities present within samples that would either be 1) considered homogeneous, or 2) would be homogenized from a standard bulk analysis. Because the process can be scaled to look at numerous microsamples within a bulk sample, it also allows the opportunity to build a larger data set showing trends in isotopic ratios and composition not possible with single average measurements from the sample. The other key result is that this work illustrates the potential for timeline improvements for obtaining initial measurements of key analytes. The process described here does not require the bulk sample to be dissolved and can proceed in parallel to that dissolution and any subsequent chemistry purification steps. Dissolution times of bulk samples can vary widely depending on the number within a batch and their mass and composition. However, we estimate that a reasonable minimum timeframe for completing this step on bulk samples is 12-24 hours following receipt and non-destructive screening. This time is representative of the likely time savings of an optimized microanalysis process before the same measurements become possible in the parallel bulk sample process.

Next steps include performing additional experiments with more post-detonation surrogate particulate samples and environmental air sample collections to further develop and test the methods with different levels of radioactive material, different matrices, and collection media. Possible sources of background introduction into the process will be carefully studied as the methods are further developed and different sample types and quantities are studied. Alternate methods to efficiently remove identified particulate from filters will also be investigated.

As described in this paper, this microanalysis-based process is part of a broader vision to automate the post-detonation analytical process where possible as well as possibly incorporate autonomy to aid in decision making at certain stages. Efforts will continue to be developed to connect the microanalysis processing steps in an automated platform. Efforts will also continue on the development of a predictive chemical model (RALF: Rapid Analytical Laboratory Flowsheet) and AI/ML assisted measurement and reporting and will be integrated with the microchemistry process to potentially provide real time process optimization.

Some of the methods that are being developed as part of this work could potentially be further developed to enable actinide measurements in the field by mass spectrometry. This also requires further development of fieldable mass spectrometers for quantitative measurement of actinides. Future work will develop methods for quantitative analysis of actinides from fieldable mass

spectrometers and couple these mass spectrometry methods to field techniques for particle collection, radiological particle identification, extraction, and counting.

Parallel efforts on improving pre-detonation nuclear material analysis through use of microanalysis will also continue and will be presented in future publications. Systematic studies are being conducted of a range of nuclear forensics properties (i.e., chemical and microstructure, morphology, elemental, and isotopics/age dating) across measurement scales on exemplar U and Pu materials. Data fusion is being used to group measurements across scales and test if properties of the bulk material can be determined from micro-measurements.

Acknowledgments

The authors thank Mathew Snow and Justin Cooper from Idaho National Laboratory for providing the surrogate particulate that is critical to demonstrate what would be possible on fresh post-detonation particulate samples.

This work was supported by the Pacific Northwest National Laboratory (PNNL) Laboratory Directed Research and Development Program and is a contribution of the Nuclear Forensics Transformational Innovation (NFTI) Initiative. A portion of the research was performed using resources available through Research Computing at PNNL. PNNL is a multiprogram national laboratory operated by Battelle for the Department of Energy under Contract No. DE-AC05-76RLO 1830.

References

1. NAS 2010. National Academies of Sciences, Engineering, and Medicine. Nuclear Forensics: A Capability at Risk. 2010.
2. Metz, L., M. Douglas, C. Beck, J. Friese, S. Herman, K. Noyes, and M. Zimmer. 2025. "Nuclear Forensics: The Ultimate Analytical Chemistry Challenge." Special Issue – Nuclear Science & Engineering 1–12. PNNL-SA-213074. DOI: https://doi.org/10.1080/00295639.2025.2592174
3. Miller, B.W., S.J. Gregory, E.S. Fuller, H.H. Barrett, B.H. Barber, and L.R. Furenlid. 2014. "The iQID Camera An Ionizing-Radiation Quantum Imaging Detector." Nuclear Instruments and Methods in Physics Research. Section A, Accelerators, Spectrometers, Detectors and Associated Equipment 767.
4. McDonald, B. S., L. Pagani, J. E. Baciak, H. S. Cunningham, B. A. Fehringer, T. W. Hossbach, M. D. Miller, H. K. Patz, R. S. Wood, and M. A. Zalavadia. 2026. "'"Microsample identification in post-detonation samples with advanced digital autoradiography systems." Journal of Radioanalytical and Nuclear Chemistry 335 (3). PNNL-SA-212646. https://doi.org/10.1007/s10967-026-10718-1
5. Patz, H. K., B. S. McDonald, K. C. Hartig, and J. E. Baciak. 2026. "Advances in Autoradiography Systems for Nuclear Forensic Analysis." Nuclear Science and Engineering 200 (4). PNNL-SA-215599. https://doi.org/10.1080/00295639.2025.2594875

6. Roach, P. J., J. Laskin, and A. Laskin. 2010. "Nanospray desorption electrospray ionization: an ambient method for liquid-extraction surface sampling in mass spectrometry." Analyst 135: 2233–2236. https://doi.org/10.1039/C0AN00312C
7. S. M. Morley et al., "Integrated Separation Scheme for Measuring a Suite of Fission and Activation Products from a Fresh Mixed Fission and Activation Product Sample," J. Radioanal. Nucl. Chem., 304, 2, 509 (2015); https://doi.org/10.1007/s10967-014-3826-2
8. S. M. Herman et al., "Evaluation of SR/TEVA/TRU Triple Stack for Separation of Activation Products," J. Radioanal. Nucl. Chem., 333, 2351 (2024); https://doi.org/10.1007/ s10967-024-09379-917
9. Mohammadhasan Dinpajooh, Niranjan Govind, Andrew M. Ritzmann, Nicolas E. Uhnak; Stability constants of lanthanide–nitrate complexes in aqueous solutions: a theoretical study. Phys. Chem. Chem. Phys. 2026; 28 (28): 17522–17545. https://doi.org/10.1039/d6cp00838k
10. Mohammadhasan Dinpajooh, Greta L. Hightower, Richard E. Overstreet, Lori A. Metz, Neil J. Henson, Niranjan Govind, Andrew M. Ritzmann, Nicolas E. Uhnak; On the stability constants of metal–nitrate complexes in aqueous solutions. Phys. Chem. Chem. Phys.2025; 27 (18): 9350–9368. https://doi.org/10.1039/d4cp04295f
11. Emmons, S., Truax, K., Lonsway, M., Pierson, B., & Archambault, B. (2026). "Peak-Based Nuclide Identification in HPGe γ - Spectrometry with Machine Learning and SHAP." *arXiv preprint arXiv:2606.14874*. https://doi.org/10.48550/arXiv.2606.14874
12. Lonsway, M. J., K. L. Truax, S. B. Emmons, B. D. Pierson, and B.C. Archambault. 2026. "Dense Autoencoders, Clustering Techniques, and Semi-Supervised Learning for HPGe Gamma-Spectra." Nuclear Instruments and Methods in Physics Research. Section A: Accelerators, Spectrometers, Detectors and Associated Equipment 1088: 171484. PNNL-SA-217987. https://doi.org/10.1016/j.nima.2026.171484
13. Lusk R, Meiers J, Bucher B, Forbush S, Carney K, Chichester DL, Snow M (2023) Retention of radionuclides in sol–gel surrogate nuclear explosive debris. J Radioanal Nucl Chem 332:683–689
14. G. Diehl et al., "Investigating Sol-Gel Matrix Loading Capacity Toward Producing Surrogate Nuclear Explosive Debris with Realistic Composition," J. Radioanal. Nucl. Chem., 333, 7, 3395 (2024); https://doi.org/10.1007/ s10967-023-09299-0
15. M. Snow et al., "Optimizing sol-gel surrogate nuclear explosive debris for laboratory analysis applications," J. Radioanal. Nucl. Chem. (2025) 334:2095–2102; https://doi.org/10.1007/s10967-025-09988-y
16. Justin T. Cooper, Tashi Parsons-Davis, Jennifer Shusterman, Todd Wooddy, Jacob Brookhart, Jessica Meiers, Thomas Holschuh, and Mathew Snow, "Quantitative Encapsulation and Homogeneity Assessment of Sol–Gel Based Nuclear Explosive Debris Simulants" ACS Applied Engineering Materials 2025 3 (11), 3804-3811; DOI: 10.1021/acsaenm.5c00555
17. Richard, N.P., Scott, S.R., Berry, C., RisenHuber, M., Munley, W., Noyes, K., Douglas, M., Metz, L. 2026. "Towards an automated approach for rapid separation of actinides using a

liquid handling system." Journal of Analytical Atomic Spectrometry, 41, 2227-2242. https://doi.org/10.1039/D6JA00127K

Table 1. Pu and Np isotopic results from large INL surrogate debris samples

Sample	^{237}Np (atoms)	±[a]	^{239}Pu (atoms) external cal.	±[b]	^{239}Pu (atoms) ID	±[c]	Δ[d]	^{240}Pu/^{239}Pu[e]	SD	^{237}Np/^{239}Pu[f]	SD[g]
^{244}Pu tracer added before dissolution											
Pu particle 1	4.07E+08	4.3%	3.99E+09	7.3%	3.89E+09	7.1%	-2.5%	0.02185	0.00045	0.1018	0.0086
Pu particle 2	4.84E+08	3.7%	7.16E+09	7.6%	7.51E+09	16%	5.0%	0.03499	0.00070	0.0676	0.0057
Pu particle 3	5.07E+08	3.7%	5.07E+09	7.4%	5.09E+09	21%	0.4%	0.02408	0.00060	0.1000	0.0083
^{244}Pu tracer added after dissolution											
Pu particle 5	2.79E+08	5.3%	2.87E+09	7.3%	1.29E+09	12%	-55.1%	0.02110	0.00049	0.0973	0.0088
Pu particle 6	2.74E+08	3.2%	2.81E+09	7.5%	2.40E+09	17%	-14.5%	0.02296	0.00081	0.0977	0.0080
Pu particle 7	4.50E+08	3.9%	4.83E+09	7.5%	3.32E+09	18%	-31.1%	0.02066	0.00037	0.0933	0.0078

[a]Uncertainties include the yield (2.9 %), standard concentration (0.92 %), and measurement RSD (1 - 4 %) at 1 sigma

[b]Uncertainties include the yield (7.1 %) and measurement RSD (2 - 3 %) at 1 sigma

[c]Uncertainties reflect the uncertainty in the measured ^{244}Pu/^{239}Pu ratio, which was dominated by signal/noise on ^{244}Pu

[d]Difference between the isotope dilution and external calibration value

[e]^{240}Pu/^{239}Pu ratios for CRM-138 measured as QC were 0.0853 ± 0.0017 and 0.0866 ± 0.0016 vs expected 0.08607

[f]^{237}Np/^{239}Pu ratios calculated from external calibration measurements

[g]Uncertainties include the ^{237}Np and ^{239}Pu atom amount uncertainties

Table 2. Uranium isotopic results from INL small particle filter

Sample	Total U recovered (pg)	$^{234}U/^{238}U$	SD	$^{235}U/^{238}U$	SD	$^{236}U/^{238}U$	SD
Sample 1	7696	0.0007510	0.0000038	0.063971	0.000039	0.0002206	0.0000018
Sample 2	1941	0.0005672	0.0000073	0.048071	0.000045	0.0001796	0.0000023
Sample 3	175	0.000420	0.000019	0.03579	0.00014	0.0001470	0.0000104
process blank	1.5						
Sample 4	6900	0.0002456	0.0000017	0.021974	0.000032	0.0001041	0.0000014
Sample 5	60	0.001159	0.000034	0.09673	0.00067	0.000307	0.000020
Sample 6	1.3						
process blank 2	0.7						

All uncertainties reported as the standard deviation (SD) of mass spectrometry measurements